

Bud Detachment in *Hydra* Requires Activation of Fibroblast Growth Factor Receptor and a Rho–ROCK–Myosin II Signaling Pathway to Ensure Formation of a Basal Constriction

Oliver Holz,¹ David Apel,¹ Patrick Steinmetz,² Ellen Lange,¹ Simon Hopfenmüller,¹ Kerstin Ohler,¹ Stefanie Sudhop,³ and Monika Hassel ^{1*}

¹Philipps-Universität Marburg, Faculty of Biology, Morphology and Evolution of Invertebrates, Marburg, Germany

²Sars International Centre for Marine Molecular Biology, University of Bergen, Bergen, Norway

³Center for Applied Tissue Engineering and Regenerative Medicine (CANTER), Munich University of Applied Sciences, Munich, Germany

Background: *Hydra* propagates asexually by exporting tissue into a bud, which detaches 4 days later as a fully differentiated young polyp. Prerequisite for detachment is activation of fibroblast growth factor receptor (FGFR) signaling. The mechanism which enables constriction and tissue separation within the monolayered ecto- and endodermal epithelia is unknown. **Results:** Histological sections and staining of F-actin by phalloidin revealed conspicuous cell shape changes at the bud detachment site indicating a localized generation of mechanical forces and the potential enhancement of secretory functions in ectodermal cells. By gene expression analysis and pharmacological inhibition, we identified a candidate signaling pathway through Rho, ROCK, and myosin II, which controls bud base constriction and rearrangement of the actin cytoskeleton. Specific regional myosin phosphorylation suggests a crucial role of ectodermal cells at the detachment site. Inhibition of FGFR, Rho, ROCK, or myosin II kinase activity is permissive for budding, but represses myosin phosphorylation, rearrangement of F-actin and constriction. The young polyp remains permanently connected to the parent by a broad tissue bridge. **Conclusions:** Our data suggest an essential role of FGFR and a Rho–ROCK–myosin II pathway in the control of cell shape changes required for bud detachment. *Developmental Dynamics* 246:502–516, 2017. © 2017 The Authors Developmental Dynamics published by Wiley Periodicals, Inc. on behalf of American Association of Anatomists

Key words: receptor tyrosine kinase; actin; Rho; myosin

Submitted 14 September 2016; First Decision 20 January 2017; Accepted 6 April 2017; Published online 15 April 2017

Introduction

Tissue morphogenesis depends on cell shape changes and requires rearrangement of the actin cytoskeleton (Burute and Thery, 2012; Levayer and Lecuit, 2012; Fagotto et al., 2013). When tissue layers or organs form from mesenchymal precursors, boundaries have to be established at which tissue separation can occur. To this end, the establishment of cortical actomyosin is required. Myosin II family members act together with F-actin to generate contractile forces which shape the new tissue, mostly by causing apical and/or apicobasal constriction of cells. Endogenous

mechanical forces may even separate cells within an epithelium when cell–cell contacts (established by E-cadherin) are weakened due to increasing binding strength between cells and their extracellular matrix (ECM) (Burute and Thery, 2012).

Formation of a bud in the freshwater polyp *Hydra* (phylum Cnidaria), constitutes an extreme case of morphogenesis, with typical dynamic changes in the transcription of different signaling pathway elements (Bottger and Hassel, 2012). *Hydra* polyps are approximately 5 mm in size, attach to the substrate with a mucous-secreting basal disk and carry an apical mouth opening on top of a tissue cone, the hypostome. Below the hypostome, a ring of tentacles equipped with specialized stinging cells, the nematocytes, serves to catch and paralyze/kill prey. Between tentacle ring and basal disk, the body column extends, which is formed by two single-layered epithelial sheets with specialized functions, including organizer formation (Hobmayer et al., 2000). Bifunctional epitheliomuscular (EM) cells form the outer

This is an open access article under the terms of the Creative Commons Attribution-NonCommercial-NoDerivs License, which permits use and distribution in any medium, provided the original work is properly cited, the use is non-commercial and no modifications or adaptations are made.

Additional Supporting Information may be found in the online version of this article.

Grant sponsor: DFG; Grant number: Ha 1732/11-1, Grant number: 1732/13-1.

*Correspondence to: Monika Hassel, Philipps-Universität Marburg, FB 17, Morphology and Evolution of Invertebrates, Karl-von-Frisch-Str. 8, D-35032 Marburg, Germany. E-mail: hassel@biologie.uni-marburg.de

Article is online at: <http://onlinelibrary.wiley.com/doi/10.1002/dvdy.24508/abstract>

© 2017 The Authors Developmental Dynamics published by Wiley Periodicals, Inc. on behalf of American Association of Anatomists

epithelium, ectoderm, and serve to shield the polyp from the surrounding medium (Buzgariu et al., 2015). They also ensure contractility in the longitudinal direction by actomyosin in basal cell processes extending along the mesogloea in the apicobasal direction (Anton-Erxleben et al., 2009). The endoderm lines the gastric cavity and its EM cells combine digestive function and circumferential contractility. Both secrete an intermitting extracellular matrix, called mesogloea in Cnidaria (Sarras, 2012).

This basal matrix has a stabilizing function by anchoring the EM cells and allows ecto–endodermal cell contacts through small pores (Shimizu et al., 2002, 2008; Seybold et al., 2016). The mesogloea is dynamically modified and degraded in morphogenetically active zones, such as the bud and tentacle region (Aufschnaiter et al., 2011). Tentacles consist of ecto- and endodermal EM cells, which reach the tentacle base zone by mass tissue movement. Here, cells undergo local rearrangement and form the regularly spaced small tentacles tubules (Hobmayer et al., 2012; Munder et al., 2013). The ectodermal EM cells transdifferentiate into battery cells and integrate stinging cells (nematocytes), which migrated actively as nematoblasts from the body column toward the tentacles (Beckmann and Ozbek, 2012).

A remarkable morphogenetically active zone is the budding zone of polyps in the mid body region. Buds evaginate in well-fed polyps by a lateral mass tissue movement, and they detach as a fully differentiated young polyp only 4 days later (Otto and Campbell, 1977). The budding process is easily observed under a dissection microscope in whole polyps due to the simple structure of the two single layered epithelia. Budding and evagination of tissue are initiated by canonical and noncanonical Wnt signaling (Hobmayer et al., 2000; Philipp et al., 2009; Nakamura et al., 2011). The evaginating tissue rearranges its actin cytoskeleton, forms a small cone and elongates by intercalation of cells to form a new body column. Complete pattern formation follows.

First, a head with a mouth opening and tentacles differentiates. Next, signaling by the fibroblast growth factor receptor, FGFRa, together with NOTCH ensures the formation of a sharp boundary between parent and bud, at which later separation occurs (Sudhop et al., 2004; Munder et al., 2010; Hasse et al., 2014). The precise mechanism by which adjacent epithelial cells are instructed to separate from each other is still unknown, but FGFR is essential: ectopic expression of HvFGFRa in a transverse row of cells causes ectopic tissue constriction and separation, even within the body column. A dominant-negative FGFRa, in contrast, is permissive for bud formation, but prohibits its detachment (Hasse et al., 2014).

A previous study indicated that FGFRa might target a pathway controlling *Hydra vulgaris* actin dynamics and/or actomyosin interactions by rearrangement of the actin cytoskeleton and formation of F-actin stress fibers at normal and ectopic separation sites (Hasse et al., 2014). It is known that during embryonic morphogenesis in Bilateria, RhoA-ROCK-myosin II-dependent pathways are often involved in regulating the actin cytoskeleton (Fagotto et al., 2013; Fagotto, 2014). Rho and ROCK are ancient signaling elements used in the prebilaterian phylum Porifera (sponges) to ensure proper morphogenesis of the aquiferous system. A connection to the actin cytoskeleton has, however, yet not been investigated (Schenkelaars et al., 2016). To elucidate whether members of the Rho, ROCK, and myosin II candidate pathway are involved in cell shape and actin dynamics during bud detachment in *Hydra*, we combined analyses of gene expression, F-actin and phosphomyosin localization with

pharmacological inhibition studies to reveal potential functions of this putative FGFR downstream pathway for bud detachment.

Results

Characteristic Cell Shape Changes Occur at the Bud Base and in the Tissue Bridge

Hydra buds evaginate in well-fed animals one at a time and detach approximately 4 days later (Otto and Campbell, 1977). Because only little morphological data describing bud detachment is available (Graf and Gierer, 1980), we prepared serial thin sections from plastic embedded, budding *Hydra vulgaris* in the early to mid stages 3, 5, 7, and in late stages 8–10 (Fig. 1, graphical overview of late bud stages in Fig. 2A). The sections revealed that between early evagination (stage 3), formation of the constriction (stage 8) and final detachment (stage 10), cells in the bud and at the bud base change their shape concomitant with changes in thickness and shape of the basal matrix, the mesogloea. In the parent and in early buds (Fig. 1A–D), the mesogloea is a thick, smooth membrane-like structure, which becomes much thinner and irregular in the body of stage 7–9 buds (Fig. 1C,D).

A detailed analysis of the detachment zone of stage 9–10 buds (Fig. 1E–I) revealed well distinguishable changes in cell shapes of the ectodermal EM cells, while such changes were not conspicuous in endodermal cells. Ectodermal cells of the bud base are very compact, and form a phalanx of apicobasally shortened cells in the prospective basal disc region (Fig. 1E–G'). Their darker staining by methylene blue (Fig. 1E–H'), which highlights nuclei and negatively charged molecules, indicates the presence of acidic vesicles or granules. In contrast, large ectodermal cells with a vacuole almost filling the cell are typical in the tissue bridge as well as in the immediately adjacent parental tissue (Fig. 1E–H').

Serial sections close to the surface of the tissue bridge revealed that these large ectodermal cells contain many vesicles in their apico-lateral parts strongly stained by methylene blue (Fig. 1G',H'). Moreover, their apical cell membranes are irregularly folded and no longer in contact with neighboring cells, slit-like gaps are visible (Fig. 1H'). The compact shape of the conspicuously short ectodermal EM cells at the bud base and the folded apical membrane of ectodermal cells in the tissue bridge suggest cell shape changes and, thus, modification of the actin cytoskeleton.

Asymmetric Accumulation of F-Actin Along the Planar Cell Axis in Bud Base Cells

Systematic analysis of the distribution of F-actin in mid and late-stage buds (Fig. 2) revealed a local rearrangement of the actin cytoskeleton concomitant with cell shape changes. In late stage 7 (Fig. 2B), the initially broad bud base constricts toward the parent. From stage 8 onward, the constriction narrows and F-actin starts to accumulate in cells of the bud base circumference with an initially poorly defined boundary (Fig. 2D–F'). In stage 10, a clear boundary has been established between bud and parent ectodermal cells, indicated by cells strongly accumulating F-actin (Fig. 2G). The bud base closes concomitant with the formation of a narrow ring of ectodermal cells (Fig. 2F,G). The boundary also sharpens on the parent's side, where F-actin accumulates unilaterally toward the separation site (Fig. 2G,H).

A slightly tilted view of the developing bud's basal disc (Fig. 2F,F') and a detailed analysis of the cLSM stack (Fig. 3) revealed several distinct cell populations in the parent and at the bud base. In parent

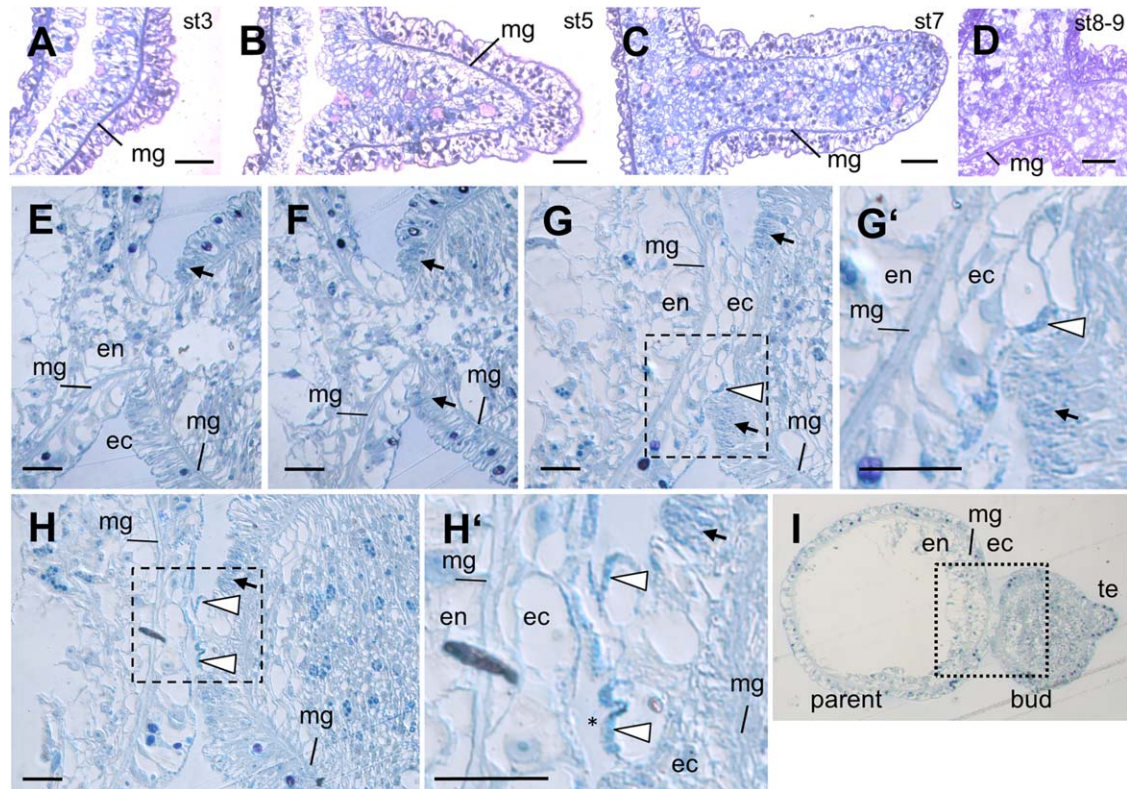


Fig. 1. Serial sections through plastic embedded *Hydra vulgaris* buds in stages 3–9. **A–D:** Longitudinal sections ($2\ \mu\text{m}$), the parent's head is oriented upward, the bud to the right. **A:** Stage 3 (early evagination). **B:** Stage 5 (early elongation, combined from two pictures). **C:** Early stage 7 (fully elongated bud with a still broad base, combined from three pictures). **D:** Stage 8–9 (constriction of bud base). **E–I:** Transverse sections ($2\ \mu\text{m}$) through the stage 8–9 tissue bridge connecting parent (left) and bud (oriented to the right). **E,F:** Sections through the tissue bridge close to the lumen. **G,G':** Section through the large epitheliomuscular (EM) cells forming the tissue bridge ectoderm and the adjacent parental ectoderm. Compact ectodermal EM cells at the bud base (black arrow). Apical vesicles (white arrowhead). **H,H':** Section at the level of the ectodermal surface of the tissue bridge. Apical vesicle accumulation (white arrow head) in the irregularly formed large EM cells, gaps develop between cells (asterisk). **G',H':** Digital close-up of (G) and (H), respectively. **I:** Section overview. Bud and parent axes are orthogonal. Therefore, the sections (E–I) through the parent are transversal, and through the bud are longitudinal. The bud body is compressed and endodermal cells are visible in all sections evoking the impression of a gastric cavity filled with cells. bt bud tip, ec ectoderm, en endoderm, mg mesogloea, te tentacle. Scale bars = $100\ \mu\text{m}$ in A–D, $50\ \mu\text{m}$ in E–H.

tissue, where the longitudinal muscle fibers of the ectodermal EM cells are well visible, cells form rosettes consisting of four to six cells in several locations. F-actin is concentrated unilaterally toward the rosette center (Fig. 3A,B) or unilaterally in cells arranging along an almost straight line instead of converging to a single center (Fig. 3A). These cells as well as those stretching out into the tissue bridge increase their diameter and often have an irregular shape, indicated by the irregular cell membranes (Fig. 3A,B).

On the bud's side, in contrast (Fig. 3C), a central cell population close to the tissue bridge has a small diameter and massively accumulates F-actin. Several of these cells, again, form rosettes of at least five cells (Fig. 3C). In the periphery of the newly forming basal disc, small cells show less cortical F-actin accumulation (Fig. 3C,D). Immediately adjacent to this central ring of cells, elongated cells stretch out along the bud body and contain a higher amount of cortical F-actin (Figs. 2G, 3D).

Shortly before detachment of the bud, the typical regular pattern of circularly and longitudinally oriented F-actin fibers in the basal processes of endodermal and ectodermal EM cells, respectively, reconstitutes along the mesogloea (Fig. 2H). At the detachment site, residual strongly F-actin-positive ectodermal cells persist for 1 to 2 hours in the parent as a wart-like protrusion with irregularly arranged F-actin fibers (Fig. 2I). Here, the circular and half-ring-like arrangement of F-actin stress fibers indicates

that ectodermal cells undergo a truly exceptional rearrangement of their actin cytoskeleton. The basal processes, usually oriented longitudinally, were not traceable in these ectodermal EM cells.

Constriction also occurs at the tentacle bases, where EM cells move into the evenly spaced tentacle tubules by mass tissue movement from the body column. Here, ectodermal cells transdifferentiate into battery cells (Hobmayer et al., 2012). In contrast to the boundary between bud and body column (Fig. 2G), F-actin does not accumulate unilaterally in the tentacle base cells (Fig. 2J–K'). Instead, the existing longitudinally oriented F-actin fibers thicken and arrange in a triangle at the intersection of body and tentacle axes (Fig. 2K').

In summary, detachment correlates with strong F-actin accumulation, formation of multicellular rosettes, and remarkable cell shape changes at the bud base, in the tissue bridge and in adjacent parental cells. These features are not observed at the tentacle bases, where EM cells just rearrange their basal processes and follow the tentacle axis.

Search for Genes Encoding Elements of a Candidate Signaling Pathway Controlling Actomyosin Dynamics and Phylogenetic Analysis of *Hydra* Rho Proteins

F-actin accumulation in cells changing their shape is a common feature and accompanies local actomyosin interactions. Very

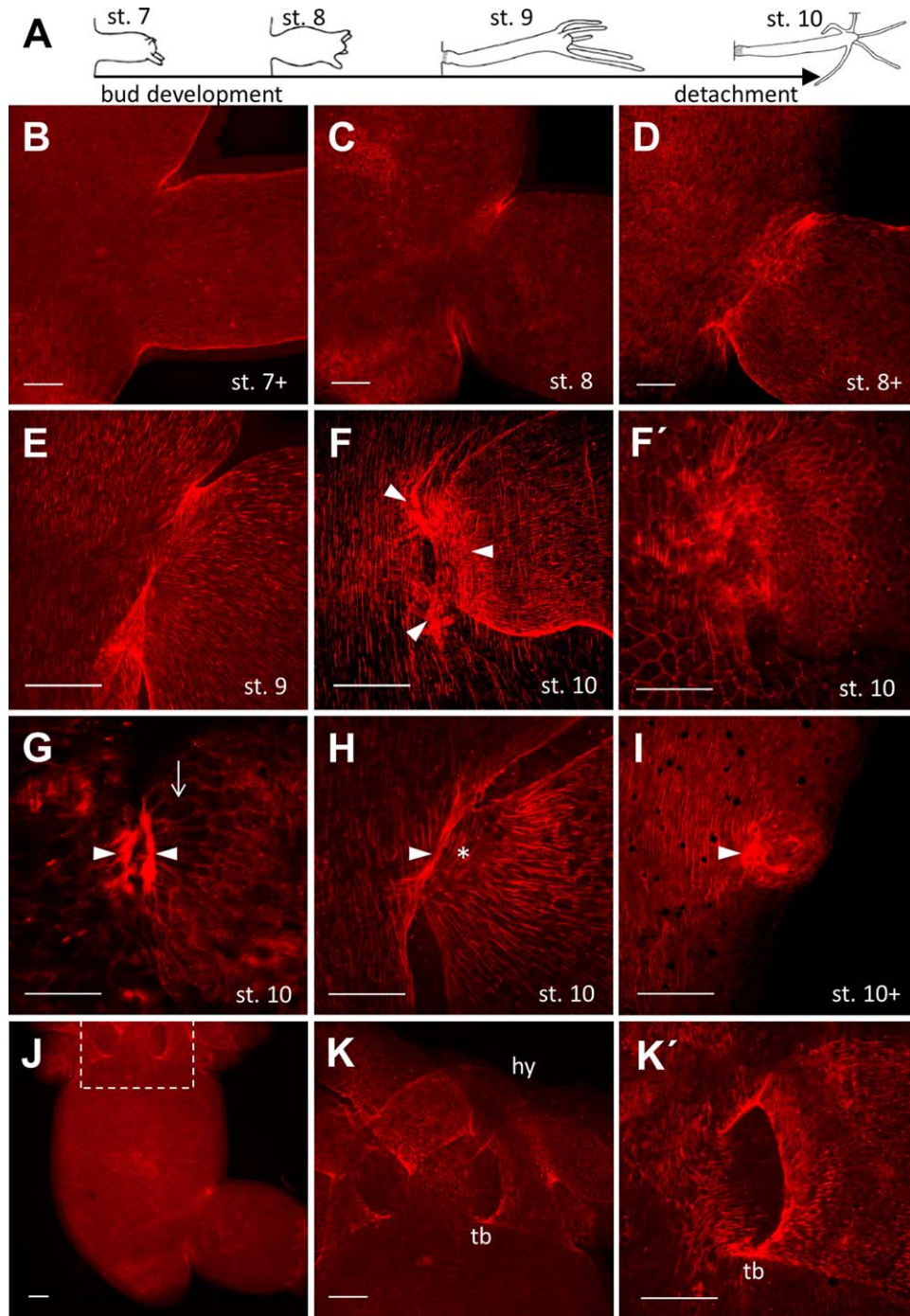


Fig. 2. F-actin accumulation at the bud base between stage 7 and detachment. **A:** Scheme of bud stages from 7 to 10 according to (Otto & Campbell, 1977). The detaching bud is not to scale. **B–K':** TRITC phalloidin staining of F-actin in *Hydra vulgaris* AEP at bud bases and detachment site (B–I) as well as at tentacle bases (J–K'). B–D: Overview stage 7+ to stage 8+. E–I: Close-up view of stage 9–10 bud bases and detachment site (I). E, F, H, I: Optical sections on the mesogloea level visualizing the normal ectodermal, longitudinal F-actin fibers. Parental as well as bud stress fibers are indicated (F, arrowheads). F', G: Optical sections closer to the ectodermal surface (lateral cell membranes visible). Actin stress fibers (arrowheads) and strongly elongated bud base cells (arrow). H: Late stage 10. Ectodermal stress fibers (arrowheads) and regular endodermal, circular F-actin fibers at the bud base (asterisk). J, K, K': Overview and close-up of the parent's head region and tentacle bases, where F-actin fibers form a triangle (open arrowhead). hy hypostome, tb tentacle base. Bud is always oriented to the right. Scale bars = 100 μm .

often, a pathway involving RhoA, Rho-associated kinase (ROCK), and myosin II is involved (Levayer and Lecuit, 2012; Schwayer et al., 2016). If this pattern is the same in bud detachment, one might expect elements of this cascade to be transcriptionally up-regulated together with *Hydra* FGFRa (Kringelchen) at the bud base.

Previously identified were a *Hydra* ROCK homologue, *HvRok* and *HmRok* (Philipp et al., 2009; Schenkelaars et al., 2016); two *Hydra* myosin II subtypes, one nonmuscular myosin (*nm_MyHC*) and a striated-type myosin (*st_MyHC*) (Steinmetz et al., 2012); three *Hydra magnipapillata* Rho-encoding genes (*HmRho1-3*), of

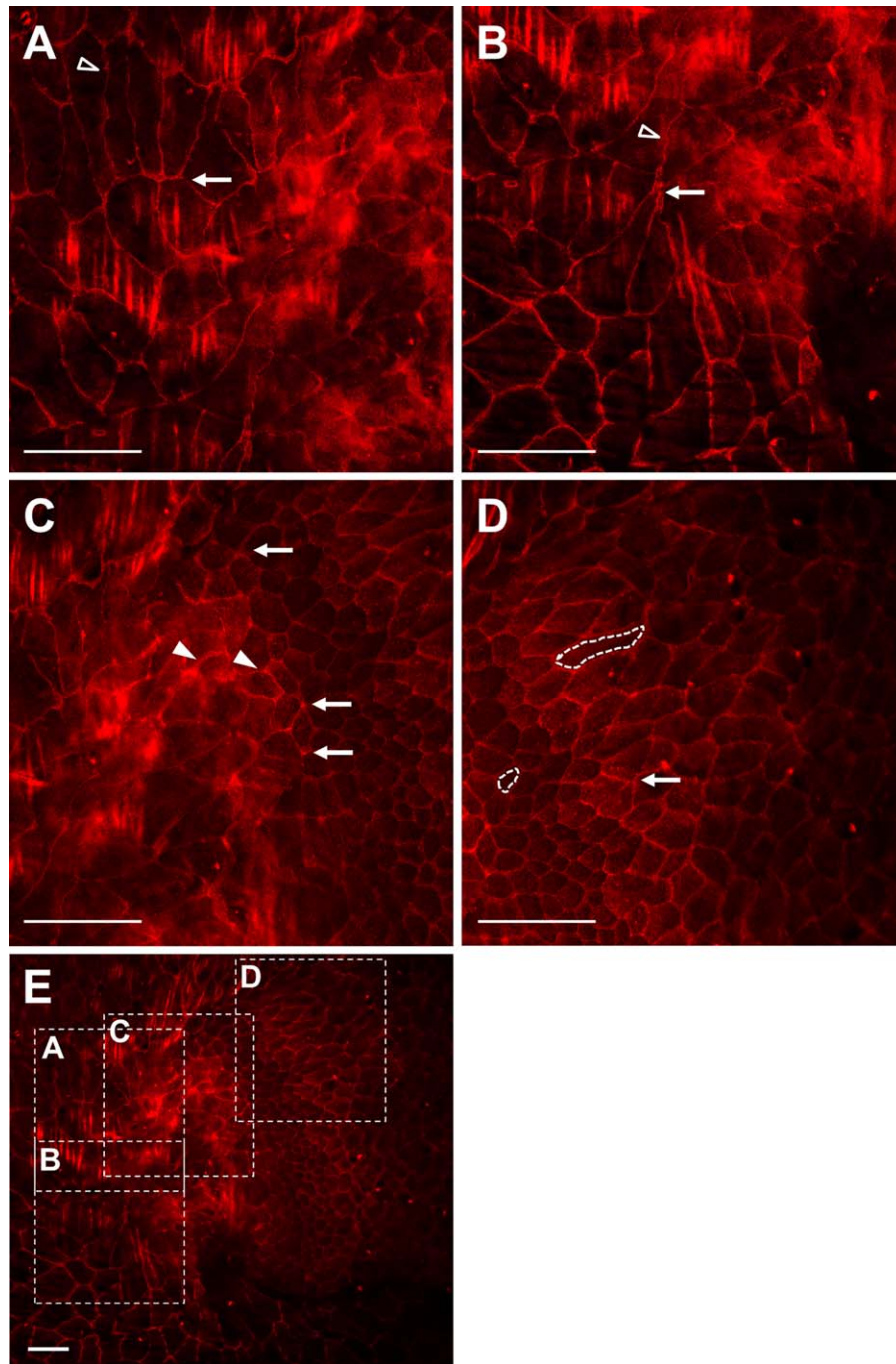


Fig. 3. Cell shape dynamics at the stage 10 bud base. Digital zoom of an optical section of the Figure 2F cLSM stack. **A,B:** Parent's side close to the bud base. A: Large, irregularly formed cells (empty arrowhead) arranged in a multicellular rosette (arrow). B: rosette (arrow) in an adjacent region, irregular cell shape (empty arrowhead). **C,D:** Bud base. C: Small central cells of the bud base immediately at the tissue bridge with strong cortical actin (arrowhead), peripheral small cells with less cortical actin forming a rosette (arrow). D: Adjacent elongated cells of the bud body with increased cortical F-actin. Dotted lines mark cell contours. **E:** Overview of the zoomed region in A–D. Scale bars = 50 μm .

which *HmRho1* and -2 were assigned to the RhoABC group (Boureux et al., 2007). Reinvestigating the current database contents, we identified a fourth *Hydra* Rho gene (*HvRho4*, Supplementary Fig. S1, which is available online), and a single gene encoding α -actinin (Supplementary Fig. S2) in the *Hydra* genome project (Chapman et al., 2010). The α -actinin is of interest for the current study, because it is an essential actin

crosslinker in stress fibers when cells change their shape and an important regulator of cell–cell and cell–matrix interactions (Foley and Young, 2014).

The *HvRho4* sequence deviates in several residues within the highly conserved GTPase and interaction domains from other Rho sequences (Supplementary Fig. S1B,C'). Phylogenetic analysis clearly assigned *Hydra* Rho1, Rho2 and Rho3 proteins as

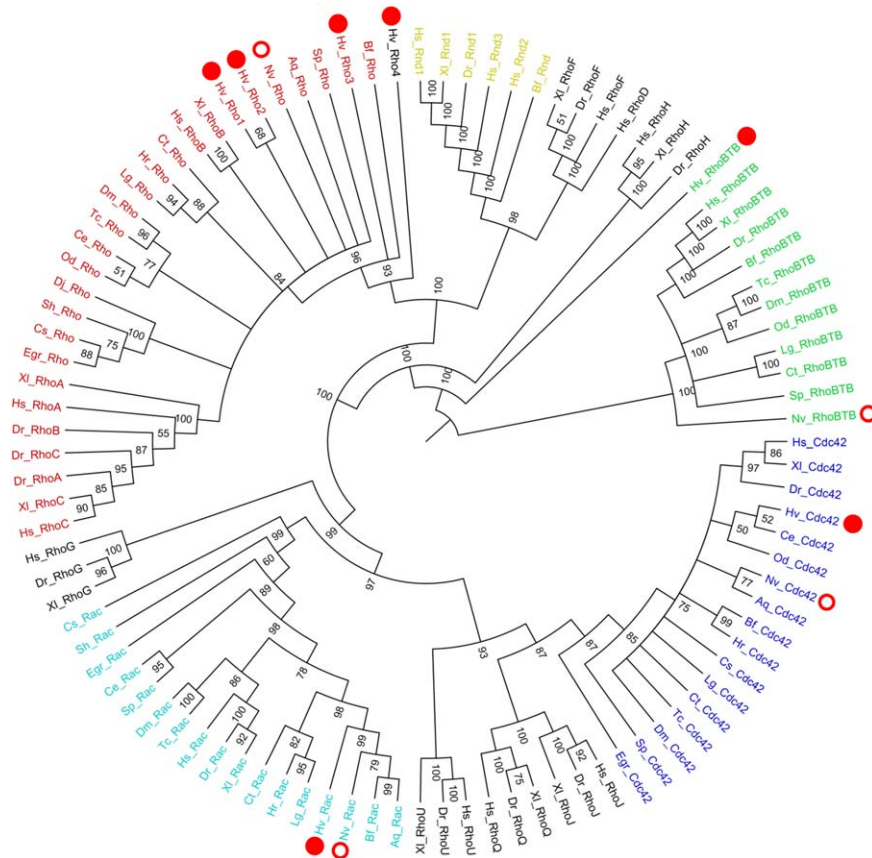


Fig. 4. Phylogenetic tree (MrBayes, MCMC) of Rho subfamilies. A, *Amphimedon queenslandica*; Bf, *Branchiostoma floridae*; Ce, *Caenorhabditis elegans*; Cs, *Clonorchis sinensis*; Ct, *Capitella teleta*; Dm, *Drosophila melanogaster*; Dj, *Dugesia japonica*; Dr, *Danio rerio*; Egr, *Echinococcus granulosus*; Hr, *Helobdella robusta*; Hs, *Homo sapiens*; Hv, *Hydra vulgaris* (red dots); Lg, *Lottia gigantea*; Nv, *Nematostella vectensis* (red circles); Od, *Oikopleura dioica*; Sh, *Schistosoma haematobium*; Sp, *Strongylocentrotus purpuratus*; Tc, *Tribolium castaneum*; Xi, *Xenopus laevis*. Accession numbers are given in Supplement Figure S1A.

orthologues to the RhoABC group, while HvRho4 was placed on an isolated branch, basal to the RhoABC family (Fig. 4). ROCK interaction sites were predicted for HvRho1 and HvRho2, but not for HvRho3 or HvRho4 (Supplementary Fig. S1B).

Taken together, a Rho-Rok-myosin II toolkit exists in *Hydra* with three RhoABC orthologues. RhoA is known to be essential in vertebrates for cell shape changes and actin regulation. For two of the *Hydra* Rhos, a ROCK binding site is predicted.

Gene Expression of *Hydra* FGFR, FGff, FGFe, and Components of a Rho-ROCK-Myosin II Candidate Pathway

Synexpression of genes often correlates with connected signaling pathways and their function (Niehrs and Pollet, 1999; Bottger and Hassel, 2012). Because the *Hydra* body consists of only two monolayered epithelia (Fig. 1), gene expression domains are easily identified by whole-mount in situ hybridization (WMISH).

The expression patterns of *HvRho1*, 2, and 3, Rok, the two myosin II genes and of *Hydra* α -actinin were analyzed in late bud stages and compared with *Hydra* *FGFRa* (*Kringelchen*), *FGFRb*, and two recently identified *Hydra* FGF-encoding genes (Fig. 5). None of the sense probes yielded a signal (not shown). All genes showed distinct zones of stronger expression in addition to weaker ecto- and/or endodermal expression along the body

column (Fig. 5). As described previously (Sudhop et al., 2004), *Hydra* *FGFRa* (*Kringelchen*) gene expression was up-regulated ectodermally at the late bud base and detachment site, where also *FGFRb* is strongly expressed (Fig. 5A,B).

In addition to a low endodermal expression in the body column, *HvRho1* mRNA was found up-regulated differentially in the ectoderm of the late bud base and in the adjacent parental tissue from stage 8 onward (Fig. 5C,C'). Neither *HvRho2* nor *HvRho3* were up-regulated at the bud base: *HvRho2* was expressed mainly ectodermally in the body column between budding region and tentacle zone (Fig. 5D), while high levels of *HvRho3* were detected in a few endodermal cells surrounding the mouth opening (Fig. 5E,E'). The *Hydra* ROCK homologue, *HvRok*, was slightly up-regulated in the parent's ectoderm cells close to the bud base extending a short distance up and down the body column (Fig. 5F,F'). For *HvRho1*, *HvRho2*, and *Rok*, an additional, very weak upregulation at the tentacle bases was observed, which is not just due to an overlay of tissues (Fig. 5C,D,F).

The two *MyHC* mRNAs (Fig. 5G-H') differed in their respective tissue localization. The nonmuscle, *nm_MyHC*, was expressed mostly endodermally, the striated-type *st_MyHC* predominantly ectodermally. Both were strongly up-regulated at the tentacle bases and the bud detachment site. *nm_MyHC* was detected in the peduncle region of parent and bud and in an additional patch of parental cells right at the detachment site, while *st_MyHC* was

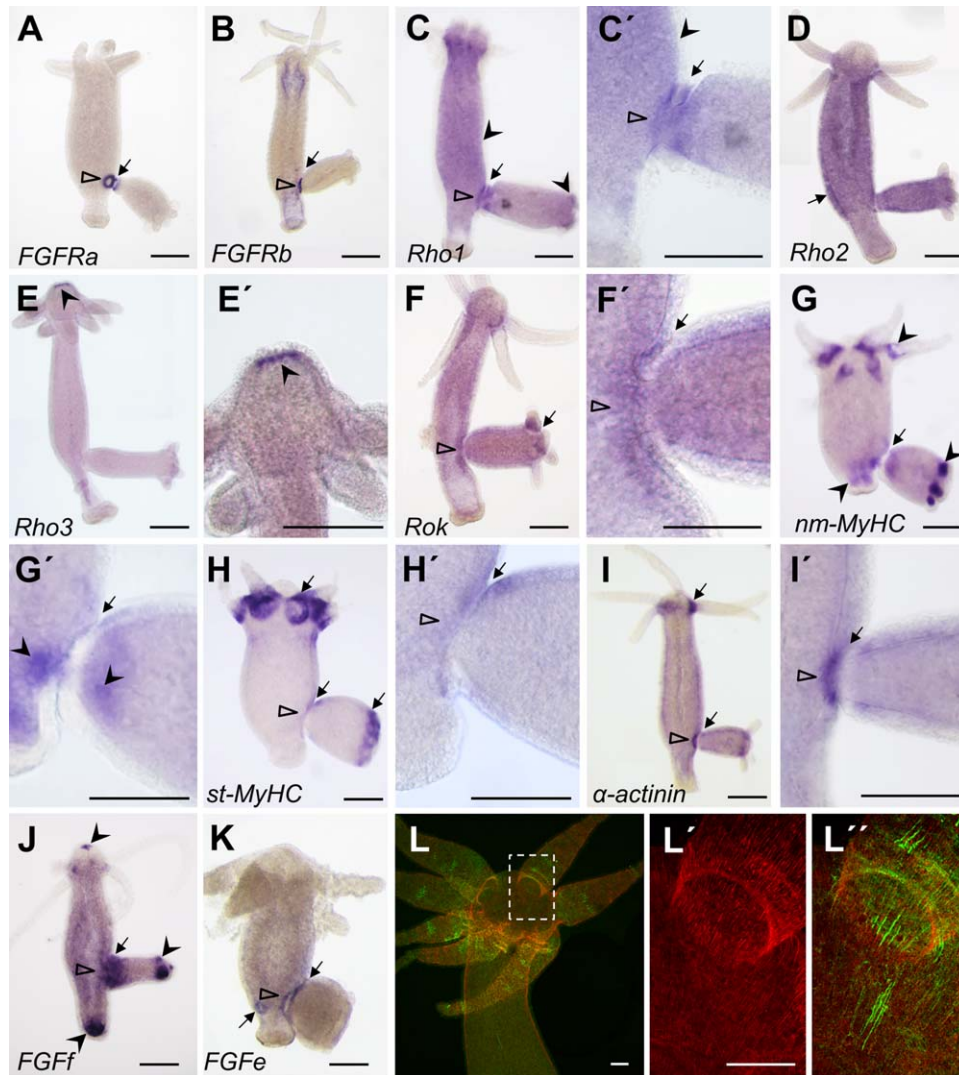


Fig. 5. A–L': Gene expression patterns of Hydra FGFRa and b, Rho1–3, ROCK, nm_MyHC, st_MyHC, α -actinin, FGff and FGFe and localization of phospho-myosin in the Hydra tentacle zone. A–G: Black arrows indicate ectodermal transcription, arrow heads endodermal gene expression and open triangles ectodermal expression in the parent close to the detachment site. A: FGFRa in a polyp carrying a stage 9–10 bud. B: FGFRb, stage 9. C, C': HVRho1, stage 9. D: HVRho2, stage 10. E, E': HVRho3, stage 10. F, F': Rok, stage 9–10. G, G': nm_MyHC, stage 10. H, H': st_MyHC, stage 9–10. The mRNA is localized asymmetrically in bud ectoderm directed toward the parent head. I, I': α -actinin, stage 9. J: HvFGff, stage 6–7. K: HvFGFe, stage 9. L–L': Immunodetection of phospho-myosin light chain (MLC20, and F-actin (TRITC phalloidin) at the tentacle bases. L: Overview, merged MLC20 and phalloidin. L': Phalloidin. L'': merged. Scale bars = 250 μ m in A–K, 100 μ m in L–L'.

localized in a ring of parental ectoderm and surrounding the bud base/peduncle region. Both myosins overlap ectodermally in a small domain at the detachment site. This domain is oriented apically, toward the parent's head (Fig. 5G',H'). Analysis of *Hv α -actinin* revealed transcriptional upregulation in parental ectodermal cells close to the bud base as well as in the tentacles bases (Fig. 5I,I').

Two potential FGFR ligands, the *Hydra* FGFR8-homologue, *HvFGff* (Lange et al., 2014) and *HvFGFe*, were detected ectodermally at the bud base with *FGff*, as described previously, being expressed endodermally also at all boundaries and termini of the polyps (Fig. 5J,K). *FGFe* expression at the detachment site parallels *FGFRa* (Sudhop et al., 2004).

In summary, both FGFRs, two FGFs, *HvRho1*, *HvRok*, *st-MHC*, and α -actinin colocalise in the parental ectoderm close to the detachment site. With the exception of *Rok* (weakly expressed)

and α -actinin (down-regulated), these genes are additionally upregulated in the bud base ectoderm. The two myosins colocalise with each other in a small domain of the bud base oriented toward the parent's head.

Actomyosin interactions require the presence of actin as well as of phosphorylated (activated) myosin light chain (MLC). Analysis of phospho-myosin localization using the MLC20 antibody revealed presence of phosphorylated MLC at the tentacle bases (Fig. 5L,M) and at the bud base (Fig. 6). Moreover, isolated fibers are visible in a scattered pattern along the body column and at the tentacle bases (Fig. 5L', below the tentacle). Controls without first antibody showed no staining (not shown). At the late bud base, actin and MLC are colocalized ectodermally (Fig. 6C–C'',F–F''). In bud stage 8–9 phospho-myosin was found strongly enriched in the central-most ectodermal bud cells, surrounding the lumen of the tissue bridge, as well as in cells of the tissue

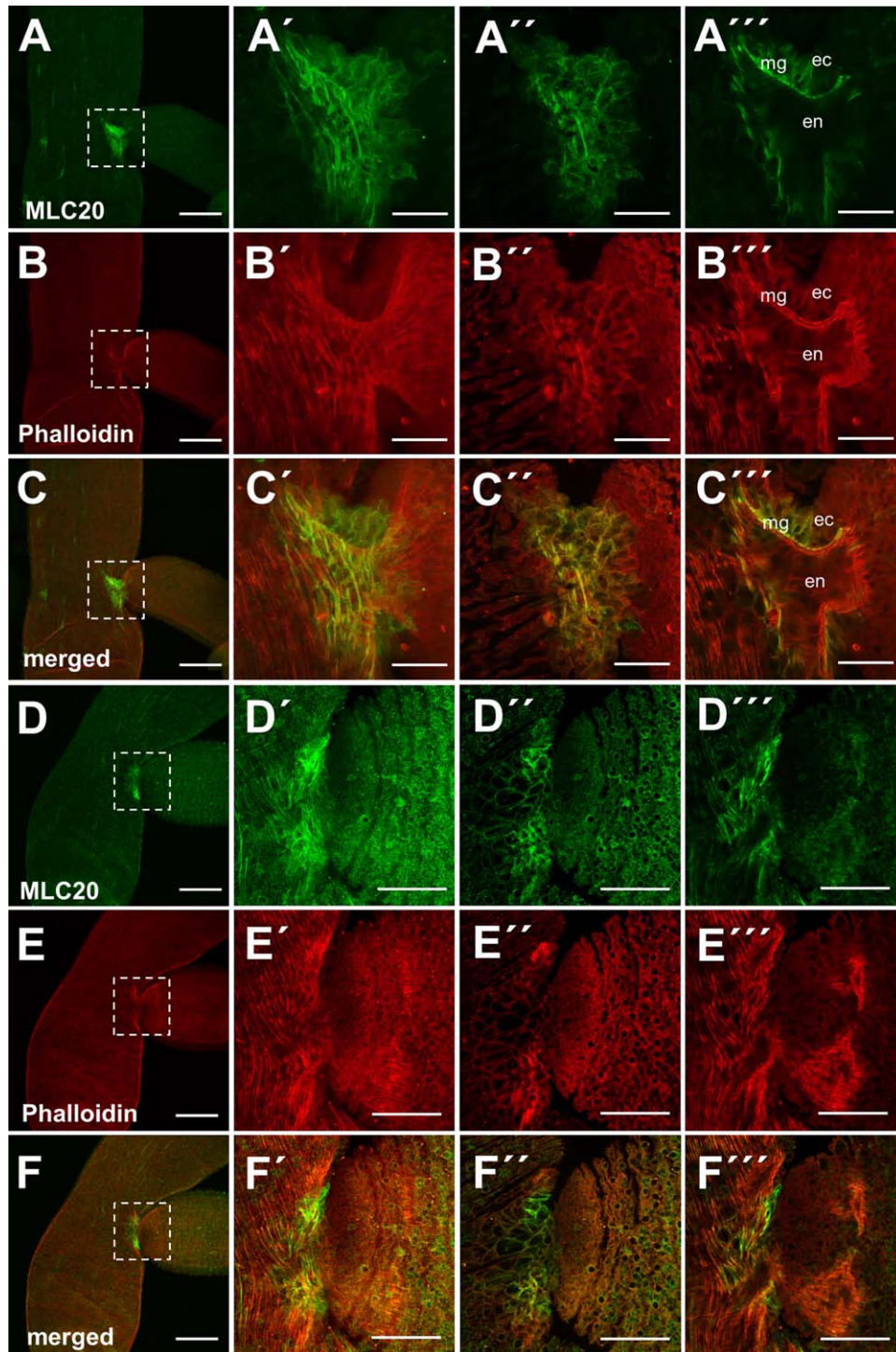


Fig. 6. A-F''': Colocalization of F-actin and phospho-myosin at the late bud base. A-E: Overview of the bud base in stage 8-9 (A-C) and stage 9-10 (D,E). The second column (A'-F') represents a maximum projection, the third column (A''-F'') shows a surface view of the tissue bridge between bud and parent, and the fourth column (A'''-F''') shows a deep view close to the lumen of the tissue bridge. A-A''', D-D''': Phospho-myosin antibody MLC20. B-B'', E-E'': TRITC-phalloidin. C-C'' and F-F'': merged. Scale bars = 250 μm in A-F first column; 100 μm in A'-F''.

bridge proper and in parental cells adjacent to the tissue bridge (Fig. 6A-A'', C-C''). In stage 9-10, phospho-myosin was detectable on the parent's side only (Fig. 6D-D'', F-F'').

In summary, all elements necessary for signal transduction through an FGF/FGFR-RhoABC-ROCK-myosin II pathway are transcribed in overlapping domains at the late bud base. Moreover,

Hv α -actinin, a protein known from other organisms to cross-link F-actin stress fibers (Sjoblom et al., 2008), joins this synexpression group. The strong and localized dynamic phospho-myosin signal at the late bud base, in the tissue bridge and in adjacent parental tissue indicates dynamic actomyosin interactions at this site.

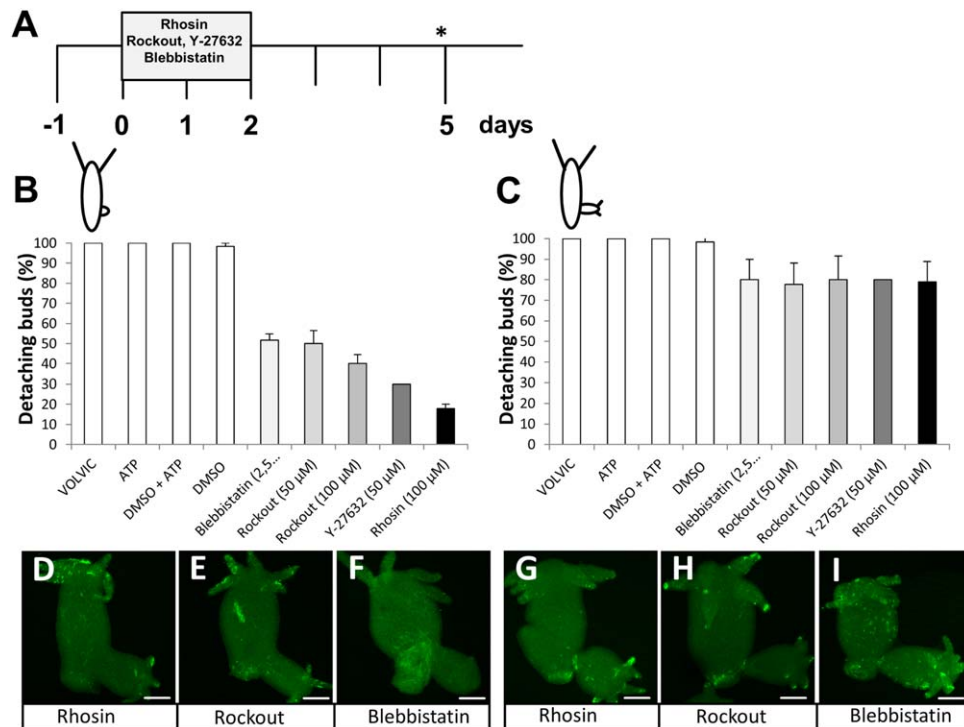


Fig. 7. Inhibition of RhoA, ROCK, and myosin II leads to failure to detach and loss of phospho-myosin. **A:** Treatment scheme. The last feeding was 24 hrs before the start of the experiment (-1). Polyps were incubated for 2 days and phenotypes evaluated and animals fixed for phalloidin and/or MLC20 staining another three days later (asterisk). **B,C:** Results of treatment of early buds (stage 3–5) (B) or late buds (stage 5–7) (C) with the inhibitors Rhosin, Rockout, Y-27632, or Blebbistatin. With the exception of the ROCK inhibitor Y-27632, all experiments were repeated at least six times with a sample size of 10 animals per inhibitor and experiment. The percentage of detaching buds and the standard error of the mean (SEM) are given. Rhosin (100 μM) (early and late buds n=90 each); Rockout (100 μM) (early and late buds n=60 each); Rockout (50 μM) (early and late buds n=60 each); Y-27632 (50 μM, early and late buds n=10 each); Blebbistatin (2.5 μM) (early and late buds n=60 each). **D–I:** Phospho-myosin (MLC20) in buds inhibited in early (D–F) or late (G–I) stages. Scale bars = 250 μm.

Pharmacological Inhibition of FGFR, Rho, ROCK, and Myosin II Prohibits Constriction at the Bud Base

A straightforward approach, by which multiple potential functions of signaling pathways can be studied in living *Hydra*, is the pharmacological inhibition of enzymes. We previously reported that SU5402, a specific FGFR inhibitor, inhibits bud detachment in *Hydra* in a similar way as *FGFRa* antisense oligonucleotides or a dominant-negative *FGFRa* (Sudhop et al., 2004; Hasse et al., 2014).

Because highly conserved protein sequences were found for the signaling elements of interest, we used well-established inhibitors against RhoA, ROCK and myosin II. In *Hydra* Rho1 and Rho2, the binding site for the RhoA inhibitor Rhosin (Shang et al., 2012) is 100% identical to the vertebrate binding site (Supplementary Fig. S1B). This site is neither predicted in HvRho3 nor in HvRho4. Two potent ROCK inhibitors, Rockout (Harding and Nechiporuk, 2012) and Y-27632 op. cit. (Kroening et al., 2010), both with unknown binding sites, were compared. Blebbistatin is a widely used inhibitor of the highly conserved myosin ATPase activity (Kovacs et al., 2004).

All four inhibitors showed effects on bud detachment comparable to SU5402. The Rho inhibitor, Rhosin, had the strongest impact (Fig. 7B). Treatment of early bud stages prohibited formation of a constriction and detachment, and 82% of buds failed to detach (Fig. 7B), while treatment of stage 5–7 buds allowed detachment of approximately 80% young polyps. Sixty percent of the polyps treated with the high Rockout concentration

(100 μM) and 50% of the ones treated with 50 μM Rockout failed to detach. Treatment with the ROCK inhibitor Y-27632 prohibited detachment in 7 of 10 polyps. Blebbistatin (2.5 μM) prevented detachment in 48% of the cases. In control incubations with DMSO less than 2% failed to detach, no effects were found with DMSO + ATP, ATP alone or using incubations with VOLVIC medium. Treatment of late buds with each of the inhibitors caused failure to detach in approximately 20% of the polyps. Toxicity of the used compounds was low or not detectable (Supplementary Fig. S3).

The phenotype generated by treating polyps carrying either early or late buds was similar to SU5402 treatment (Sudhop et al., 2004; Hasse et al., 2014). Young buds later formed a broad tissue bridge, while further developed buds formed a narrow one (Fig. 8). No phospho-myosin was detected at the base of nondetaching, early-treated buds (drug exposure as in Fig. 7A), even 3 days after the end of treatment (n = 10 each; Fig. 7D–F). A variable pattern of scattered single phospho-myosin-positive fibers was found in the body column (particularly following Blebbistatin treatment) and in tentacles. The phospho-myosin-positive fibers colocalized with actin fibers (similar to Fig. 5L'). A weak phospho-myosin signal appeared at the bud base of polyps treated in late bud stages (n = 10 each, Fig. 7G–I).

Detection of F-actin in the branched polyps resulting from treatment of early buds (Fig. 8) revealed a triangular alignment of actin fibers at the intersection of parent tissue and the broad tissue bridge to the bud (Fig. 8A–C'). This F-actin triangle resembles the one detected at the tentacle bases (Fig. 2K') and indicates that

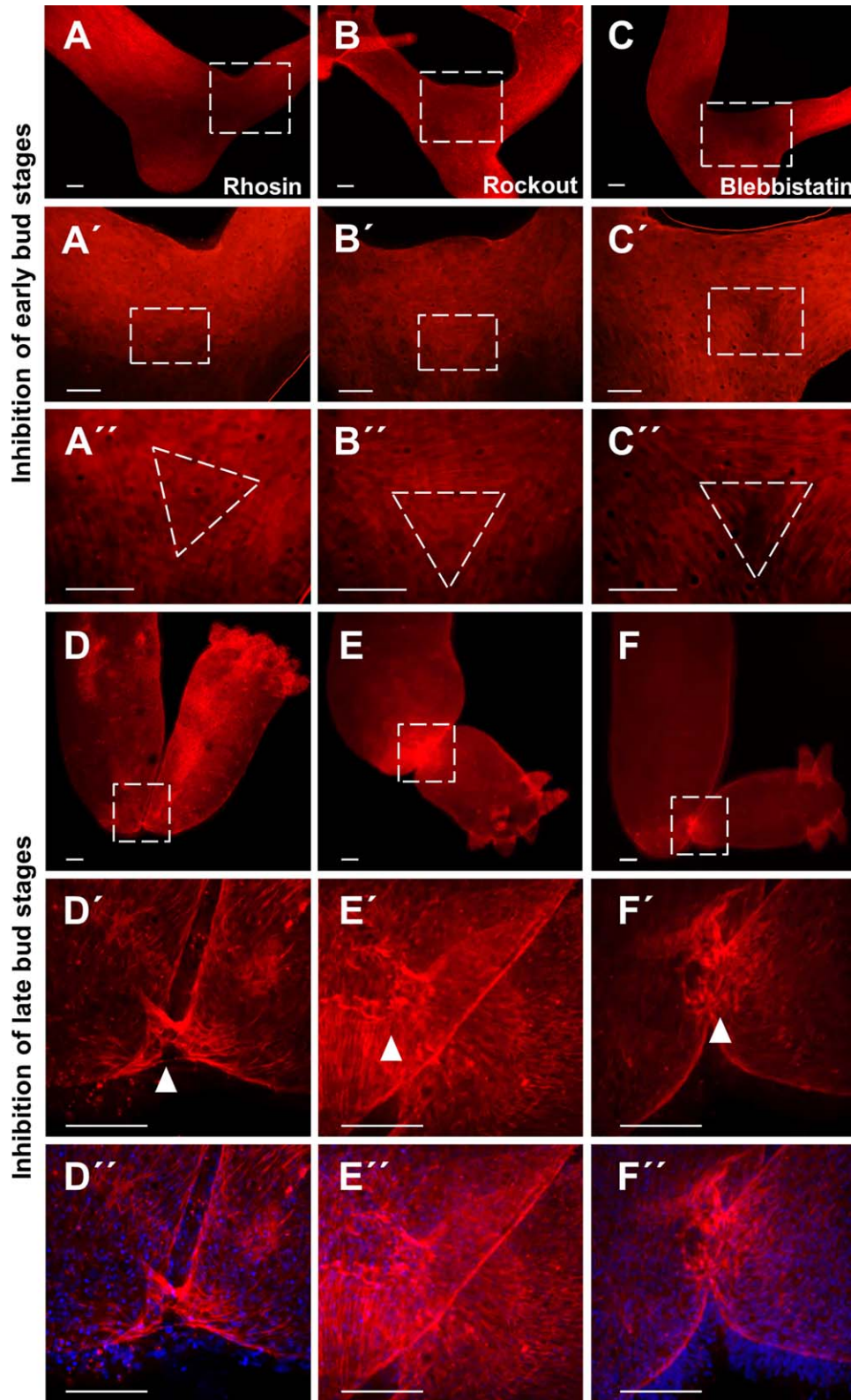


Fig. 8. TRITC-phalloidin staining of early and late budding *Hydra vulgaris* AEP treated with either Rhosin, Rockout or Blebbistatin. *Hydra vulgaris* AEP (stage 3–5) were subject to inhibitor treatment as indicated in Fig. 7. **A–C'**: Inhibitors: Rhosin (RhoA-specific inhibitor) (A–A'), Rockout (Rho kinase inhibitor) (B–B'), Blebbistatin (myosin II ATPase inhibitor) (C–C'). Treated buds fail to detach and remain attached to the parent with a broad tissue bridge as Y-shaped, branched animals for weeks. A'–A': The higher magnifications of the branching area shows a triangle of actin filaments at the intersection of parent and bud tissue (A', B', C') (close-up in A', B', C'). **D–F'**: Pictures of phenotypes obtained in the experiment leading to Figure 7C. D', E', F': TRITC-phalloidin (red) and DAPI (blue) staining. Treatment of bud stages 5–7 with Rhosin (D–D'), Rockout (E–E'), or Blebbistatin (F–F') resulted in narrow tissue bridges (white arrowheads) persisting between bud (oriented to the right) and parent. Scale bars = 10 μ m in A–C'; 100 μ m in D–F.

the EM cells are unable to rearrange their actin cytoskeleton circumferentially along the bud base, if any of the FGFR, Rho-ROCK-myosin II candidate pathway components is inhibited. Instead, the orientation of the F-actin fibers follows and reflects the new orientation of the EM cells along the bud's axis. In late buds (Fig. 8D–F'), a chaotic arrangement of F-actin fibers indicates failure to arrange them properly for final detachment.

In summary, the Rho, ROCK and myosin ATPase inhibitors evoke a morphological phenotype indistinguishable from the FGFR inhibitor SU5402. While phospho-myosin is not detectable in the broad tissue bridges resulting from treatment of early buds, a patch of cells positive for the activated myosin occurs ectodermal at the base of buds treated late.

Discussion

Tissue separation in embryonic systems occurs mostly by mechanical forces generated by apical constriction of cells, which is mediated by actomyosin interactions and often controlled by a pathway using RhoA, ROCK, and myosin (Fagotto, 2014). In *Drosophila*, for example, apical constriction of cells along the midline is essential to internalize gastrulating tissue (Martin et al., 2009). Concomitant with apical constriction the diameter of the central cells decreases, while mechanical tension increases the diameter in cells positioned lateral to the invagination zone (Martin and Goldstein, 2014).

We will discuss similar asymmetric cell shape changes at the *Hydra* bud base and the role of a candidate pathway by means of Rho, ROCK, and myosin II.

Functional Importance of Cell Shape Changes at the Bud Base and in the Tissue Bridge

The occurrence of very small and compact cells at the *Hydra* bud base and large cells with irregular cell membranes in the parent and the tissue bridge resembles similar cell shape and size differences observed during *Drosophila* gastrulation (Martin et al., 2009). Moreover, development of multicellular rosettes, as also found in *Drosophila* (Blankenship et al., 2006), indicates mechanical forces at the detachment site. Tissue sections and phospho-myosin distribution, however, suggest that the mechanisms underlying cell shape changes in *Hydra* are not identical to the ones controlling tissue invagination in *Drosophila*.

In contrast to fly gastrulation, the central bud cells close to the tubular tissue bridge are very small and not just apically constricted. The strong accumulation of F-actin in these cells suggests apicobasal additional to apical and/or lateral constriction. A recent study showed that the ability for apicobasal shortening is an intrinsic property of fully differentiated basal disk cells. It is caused by an apicobasally oriented, intracellular F-actin fiber (Rodrigues et al., 2016). Intracellular apicobasal F-actin fibers would be perfectly suited to weaken cell–matrix interactions at the separation site, when, at the same time, adjacent cells increase their binding to the matrix as in vertebrate tubulogenesis (Burute and Thery, 2012). Whether a change in cell–cell vs. cell–matrix interaction is necessary for bud detachment is an interesting question for future mechanistic studies.

The increase in volume and the apical vesicle accumulation of the exceptionally large, vacuolized EM cells covering the tissue bridge and the adjacent parental body column also distinguishes bud detachment from gastrulation processes. The function of the

large cells is unknown, but some speculations may be allowed. Cell enlargement plus vacuolization might serve to passively loosen the tissue bridge and adjacent parental tissue for detachment. Accumulation of apical vesicles, F-actin, and, particularly, of phospho-myosin suggest, however, that these cells contribute actively. We propose three functions for the tissue bridge cells.

First, apical vesicles in EM cells of the body column are known to release glycocalyx components (Bottger et al., 2012). When tissue-bridge cells separate (Fig. 1), a new glycocalyx might be required, either to stiffen the tissue bridge for detachment by sphincter contraction of the bud base (Takahashi et al., 1997) or to enable reintegration of the cells into the body wall following detachment. Cell reintegration has not been investigated in detail, but the detachment site remains morphologically visible for 1–2 hr, in which *FGFRa* expressing cells are detectable in a small, contracting ring and finally in a patch (Sudhop et al., 2004) similar to *FGFe* (Fig. 5K). This coexpression will allow to identify the reintegrating, shrinking cells in future studies.

Second, the coexpression of the matrix metalloprotease *MMPA-3* with *FGFRa* at the bud base and detachment site (Münder et al., 2010) raises the possibility that the large cells secrete MMPA-3, which digests extracellular matrix components in the mesogloea to enable detachment. Third, the final detachment signal is given by myoactive peptides, which activate a sphincter contraction and shedding of the bud (Takahashi et al., 1997). The large cells might contribute to detachment by using their actomyosin to stiffen the tissue by, like in *Drosophila* (Blankenship et al., 2006), forming rosettes, and perhaps supported by an altered glycocalyx.

Taken together, the functions of the small bud base cells as well as of the large cells have to be investigated in detail to elucidate, how the detachment process is finalized.

Role of Ecto- and Endoderm During Tissue Separation

Phospho-myosin was detected in ecto- but not in endodermal cells at the late detachment site, suggesting a leading role for the ectoderm in tissue separation. This feature, interestingly, supports our previous observation, that tissue separation occurs with different kinetics when *FGFRa* (Kringelchen) is ectopically expressed ecto- or endodermally in transgenic polyps (Hasse et al., 2014). Ectodermal, ectopic Kringelchen-GFP induced a rapid and complete tissue separation within approximately 4 days, corresponding to bud detachment. Endodermal ectopic expression, on the other hand, resulted in a relatively quick endodermal separation, while autotomy of the body column took at least 10 days. Thus, coordination between ecto- and endoderm is possible, either by physical contacts of cells through the mesogloea pores (Shimizu et al., 2008), or by diffusible molecules like FGFs. Whether *FGFRa* acts effectively in both epithelia or whether *FGFRb* (Rudolf et al., 2013) assists in tissue separation has to be analyzed as well as the roles of *FGFf* and *FGFe*.

In this context, the predominant expression of the two myosin II genes, *st_MyHC* and *nm_MyHC*, in ecto- and endoderm, respectively, is interesting. Their differential expression could be correlated, as in many bilaterians, to the contraction speed of the respective EM cells (Steinmetz et al., 2012). While the *st_MyHC*-expressing, ectodermal cells contract relatively fast (e.g., as escape response after touching), the circular muscle cells expressing *nm_MyHC* contract slowly (predominantly during peristalsis). We found no evidence for the presence of more than two myosin

II genes in *Hydra*. The two myosins are thus not used exclusively for muscle functions in the basal myonemes of the EM cells, but they also function in actomyosin interactions driving cell shape changes.

Given its ectodermal expression, the striated-type, st_MyHC, may be more relevant for tissue separation than the predominantly endodermal nm_MyHC. However, nm_MyHC transcription is also upregulated ectodermally close to the detachment site. Recently, *Drosophila* nonmuscle myosin II has been reported to be the essential component for the rate determination of tissue folding (Vasquez et al., 2016). The evaluation of *Hydra* myosin II protein localization and function is necessary to decide this issue.

A Rho–ROCK–Myosin II Candidate Pathway

Ectopic expression of FGFR α causes ectopic tissue separation and targets two pathways: first, a MAPK–dpERK pathway in parental cells close to and within the tissue bridge; second, in a different cell population, a pathway causing F-actin accumulation in cells at the bud base and at ectopic separation sites (Hasse et al., 2014). We, therefore, used gene expression analysis and inhibitor studies to investigate whether a Rho–ROCK–myosin II signaling pathway is required for cell shape changes during bud detachment, and whether it has a link to FGFR signaling. *Hydra* Rho1, 2 (Supplementary Fig. S1B'), Rok (Philipp et al., 2009; Schenkelaars et al., 2016), and the two myosins II (Steinmetz et al., 2012) are structurally conserved to their bilaterian counterparts and, therefore, expected to perform similar functions.

Although physiological side effects of the used inhibitors cannot be excluded, the phenotype of nondetaching buds was consistent with the expression of Rho1, Rok, and the two myosins II.

The fact that drug exposure resulted in a scattered (if any) phospho-myosin pattern in the broad tissue bridge of nondetaching buds likely indicates the presence of normal body column tissue. In contrast, presence of phospho-myosin in the small tissue bridges of buds treated late, suggests that failing detachment is due to the chaotic arrangement of their F-actin fibers (Fig. 8), which might prohibit a coordinated sphincter contraction.

Synexpression with the two *Hydra* FGFRs, two FGFs and α -actinin as well as a phenotype identical to FGFR inhibition suggest a functional relationship between FGFR and the Rho, ROCK, and myosin II pathway. Its function for bud detachment appears equally important as FGFR signaling.

The existence of three members of the RhoABC subgroup turned out interesting. Their sequence features and differential expression indicates that *HvRho1* is the most likely candidate to act within the pathway: Rho1 and Rho2 sequences contain a ROCK-binding site and the interaction site for the Rhosin inhibitor, but only Rho1 is up-regulated at the bud base.

Rho2, expressed in the body ectoderm, might control cell shape changes along the body column, and Rho3 (neither ROCK- nor Rhosin-binding sites), which is expressed in a small cell population surrounding the mouth, might be necessary for shape changes required in the very flexible mouth opening. This function would also be essential at the tentacle base to control the cell shape changes leading to tissue constriction and tubular protrusions. The weak upregulation of Rho1, 2, and Rok at the tentacle bases raises doubts whether the same pathways are active at the bud and tentacle bases, but protein level investigations are missing. There certainly is an additional level of regulation at the bud base, which ensures detachment additional to constriction.

An amino acid exchange in the predicted Blebbistatin binding site of st_MyHC is interesting under functional aspects as it raises the possibility that Blebbistatin interacts differentially with the two *Hydra* myosins II. In *Dictyostelium* myosin II four residues, Ser456 (or Ala), Thr474, Tyr634, and Gln637 are essential for binding the inhibitor (Allingham et al., 2005). These residues are identical in the *Hydra* nm-MyHC. In st-MyHC the position of Tyr634 is changed to a His. Allingham and coauthors showed that replacement of Tyr634 by Phe in skeletal muscle myosin, in myosin Va, and in myosinX increases the $IC_{50} > 150 \mu\text{M}$ and abolishes specificity. Whether the exchange of Tyr to His in *Hydra* st-MyHC causes a decreased affinity to Blebbistatin, has to be investigated by biochemical studies and is essential to decide, which MyHC is essential for detachment. Similar effects and time courses of the inhibitors of FGFR and of the candidate pathway elements suggest a close relationship between them.

A Signaling Network Might be Active at the Bud Base

Invagination during *Drosophila* gastrulation is completely reversible, when the PI(4,5)P₂ level is experimentally manipulated (Guglielmi et al., 2015). PI(4,5)P₂ is an essential phospholipid, located in the apical domain of the cell membrane and one of the essential elements controlling cell polarity. Upon activation of FGFR, G-protein coupled receptors (GPCR) or noncanonical Wnt signaling (Dailey et al., 2005; Seifert and Mlodzik, 2007), PI(4,5)P₂ is hydrolyzed by phospholipase C γ (PLC γ) yielding the second messengers diacylglycerol (DAG) and IP₃ and activate pathways targeting the actin cytoskeleton.

An involvement of inositol phospholipids in *Hydra* bud detachment is possible as deduced from the fact that lithium ions prevent bud detachment and that this effect is correlated with remarkable changes in the inositol/inositol phosphate levels consistent with the inhibition of inositol mono- and bisphosphatases (Hassel and Berking, 1990; Hassel and Bieller, 1996). Inositol phosphatases ensure inositol recycling, which is essential for the synthesis of inositol lipids, like, PI(4,5)P₂. Although LiCl is best known as an activator of canonical Wnt signaling (by inhibiting GSK3 β), there is no evidence that canonical Wnt signaling affects bud detachment (own unpublished observations). Noncanonical Wnt signaling, in contrast, which controls bud and tentacle evagination (Philipp et al., 2009) and regulates cell polarity and directed migration in planar polarity signaling in general (for a review see Seifert and Mlodzik, 2007), is able to target the actin cytoskeleton by means of Rho, or by means of a PI(4,5)P₂/PLC pathway, just like FGFR (Dailey et al., 2005). In *Hydra*, *Wnt8* is expressed at the bud base (Philipp et al., 2009), opening the possibility that noncanonical Wnt signaling acts in a network with FGFR and Rho–ROCK–Myosin II.

Conclusions

Despite the possibility that multiple signaling pathways converge on the actin cytoskeleton, we consider it most likely that FGFR signaling plays the major role in the activation of ectodermal Rho–ROCK–myosin II signaling in *Hydra* bud detachment. This conclusion is supported by previous experiments which revealed a direct effect of ectopic FGFR on ectopic F-actin accumulation and tissue separation. It is further supported by the ectodermal synexpression of two FGFs, both FGFRs, Rho1, ROCK, and non-muscle as well as striated-type MyHC at the detachment site. If

and how endodermal cells contribute to detachment remains an open and interesting questions.

Experimental Procedures

Hydra culture, timing of bud stages and WMISH were performed as described previously (Grens et al., 1996; Sudhop et al., 2004). *Hydra vulgaris* AEP was used throughout the study unless otherwise indicated. For in situ hybridization, sequences for *Hydra* myosin (*nm_MyHC*: XP_012560866; *st_MyHC*: XP_002157926.3), *Hv_α-actinin* (XP_004208576.1), *Hv_Rho1-3* (Supplementary Fig. S1), *HvRok* (NM_001309671.1), the extracellular-domain-encoding sequences of *FGFRa* (XP_002157656) and *FGFRb* (XP_002157686), *HvFGFf* and *HvFGFe* were used to synthesize digoxigenin (Dig) - labeled RNA sense and antisense probes (Dig-labeling system, ROCHE). The quality of RNA probes was verified by Northern blotting and approximately 300 ng of the respective RNA probe per 0.1 ml was used for standard WMISH.

Deviating from this protocol, proteinase K digestion was prolonged for *Hydra vulgaris* AEP from 10 to 15 min and in situ hybridization required an additional 1:100 (*FGFe* and the two myosins) or 1:5 (*Hv_α-actinin*) dilution of the probe. In case, the in situ hybridization signals in *Hydra vulgaris* AEP were weak (*α-actinin*, *FGFf*), we used *Hydra magnipapillata* or *Hydra vulgaris*, Zürich, polyps, which yield a better signal-to-noise ratio, as shown previously (Lange et al., 2014). The pattern remained similar. Color development was performed at room temperature and allowed to proceed for 5 to 30 min (*Rho1*, *myosins*, *FGFRs*, *FGFe*, and *α-actinin*) or for up to 3 hr in the dark. All animals (3 to 5 per experiment) showed the same expression pattern.

Tissue Sections, Detection of F-actin/DAPI by Phalloidin, and of Phospho-myosin by MLC20 Antibody Staining

Tissue sections were prepared from normal animals as described (Sudhop et al., 2004) and stained with 1% methylene blue. Whole-mount tetramethylrhodamine (TRITC)-phalloidin and DAPI (4',6-diamidino-2-phenylidole-dihydrochloride) staining was performed as described previously (Hasse et al., 2014). For phospho-myosin staining, animals were relaxed in 2% urethane for 1 min and fixed overnight in 4% paraformaldehyde (PFA) in 1 × phosphate buffered saline (PBS), pH 7.4 (0.15 M NaCl in 0.01 M sodium-phosphate buffer) at 4 °C. Polyps were washed and permeabilized 3 × 20 min in 1 × PBT (1 × PBS containing 0.25% Triton X-100, v/v). Polyps were incubated for at least 7 hrs in blocking buffer (1 × PBT containing 2% BSA). The primary antibody (polyclonal MLC20 (Myosin light chain -phospho S20), Abcam) was diluted 1:400 in blocking buffer and incubated overnight at 4 °C. Following 3 × 20 min washing steps in blocking buffer, 3 × 10 min in PBT and again 3 × 20 min in blocking buffer at room temperature, the animals were incubated for 2 hr at room temperature with the secondary antibody (FITC-Affinity Pure goat anti-rabbit (Sigma), diluted 1:750). Unbound antibody was removed by washing 6 × 20 min in PBT followed by an overnight washing step in 1 × PBS, pH 7.4 at 4 °C. For MLC20/TRITC-phalloidin double staining, TRITC-phalloidin was incubated in washing buffer for 1 hr following the first washing step. The remaining five washing steps were performed as detailed above. Specimen were embedded in Roti-Mount-Fluorocare and

polymerized in the dark. Images were taken on a confocal laser scanning microscope, Leica TCS SP5.

Incubation With Inhibitors

Inhibition with SU5402 (Calbiochem) was performed as described (Sudhop et al., 2004). Optimal concentrations were determined based on published data by evaluating the strongest effects on *Hydra* at low toxicity (Supplementary Fig. S3). For inhibition with Rhosin (Calbiochem, [Shang et al., 2012]) at 100 μM, Rockout (Calbiochem, [Harding and Nechiporuk, 2012]) at 50 and 100 μM; Y-27632 at 5, 20 or 50 μM or Blebbistatin (Sigma, [Kovacs et al., 2004; Fagotto et al., 2013]) at 2.5 μM, stage 3–5 or stage 5–7 buds (Otto and Campbell, 1977) were selected 24 hrs after the last feeding. Polyps were incubated at 18 °C in the dark for 48 hrs in commercially available VOLVIC mineral water containing a final concentration of 1% dimethylsulfoxide (DMSO), 1 mM adenosine triphosphate (ATP) and the corresponding concentration of an inhibitor. As controls, we used untreated polyps carrying the respective bud stages as well as animals incubated in the DMSO/ATP solute without the respective inhibitor. Phenotypes were evaluated 3 days after the end of treatment, when normal buds have detached. Experiments with Rhosin, Rockout, and Blebbistatin were repeated at least six times independently (Rhosin 9x) with a sample size of 10 animals per inhibitor treatment. Y-27632 treatment was carried out once with 10 animals for comparison.

Database Search and Phylogenetic Analysis

To reveal the Rho sequences in *Hydra*, we explored the NCBI databases (<http://www.ncbi.nlm.nih.gov/>). Annotated human Rho sequences (NP_001655.1 (RhoA), CAA29968.1 (RhoB), AAM21119.1 (RhoC)) were used as query to identify similar sequences in *Hydra* and other animals. The deduced *Hydra* protein sequences were aligned with available protein sequences of the poriferan *Amphimedon queenslandica*, the cnidarian *Nematostella vectensis*, Platyhelminthes, Mollusca, Annelida, Insecta, and Chordata as indicated. Sequences were predicted by automated computational analysis (genomic sequence annotated using gene prediction method: Gnomon, supported by EST evidence). ROCK binding sites in the HvRho proteins were predicted by the NCBI function “Identify conserved domains”.

For the phylogenetic tree, sequences were aligned using ClustalX 2.1 (Jeanmougin et al., 1998) with BLOSUM30 alignment matrix and unrooted trees were derived using a Metropolis-coupled Markov Chain Monte Carlo (MrBayes 3.2, ngen=1000000, samplefreq=100). Trees were displayed using FigTree v1.4.2.

RNA Isolation, cDNA Synthesis, and PCR of Sequences of Interest

The Quickprep Micro Kit (Amersham) was used to harvest poly(A)⁺ RNA from *Hydra vulgaris* AEP. Poly(A)⁺ RNA was reverse transcribed using Revert Aid TM Premium First-strand cDNA Synthesis Kit (Fermentas) and diluted 1:100 before PCR amplification of the genes of interest. *Hydra nm_MyHC*, *HvRho*, *HvRok*, and *Hv_α-actinin* gene sequences were PCR amplified using the following primer pairs: Primers for *st_MyHC* as in (Steinmetz et al., 2012) *nm_MyHC* forward: AGCTGCGTTGCCGATAATA,

reverse: CGTTGTTGTGCTTCTGCCAA; *Hv_α-actinin* forward: TGATCCAGCATGGGAAATGC reverse: ACTGGGCGATTGCTTAA TCG; *Hv_Rok* forward: AACTGCTGTTGGCACTACT, reverse: ATCTGCAACAGCTTGGGCTT; *HvRho1* forward: ATTGTTGGTGA TGGTGCTTGTGG, reverse: GCAGCTCTAGTTGCAGTTTCAAATA CC; *HvRho2* forward: GCAATTCGCAAGAAATTAGTC; reverse: GCCATCTCACGACCTTGTCAATC; *HvRho3* forward: GAAATCA TCAGAGAGAAGCCC, reverse: TGATATCTTCGAGGTCACGCT. Amplified cDNA fragments were AT-cloned into the pGEM T-Easy vector (Promega). Clone identity was confirmed by sequencing (SeqLab). Promoters used for anti-sense transcription were T7 or SP6 depending on the orientation of the blunt-ended cloned cDNAs.

Statistics

In Figure 7, the error bars indicate the standard error of the mean (SEM), which is the standard deviation of the sample mean's estimate of a population mean. The SEM was calculated using the Excel program (Bland and Altman, 1996).

Acknowledgments

We thank two unknown referees for critical comments which improved the manuscript and Eva Frei for polishing the manuscript. Heide Brandtner and Marcel Hemming did an excellent job in caring for our *Hydra* cultures. We are indebted to Helga Kisselbach-Heckmann and Lothar Beck for help with the thin sections. The FGFRb in situ hybridization was performed by Alexander Becker and Dominic Grauer in our MSc course. Without support by the DFG grant HA1732/13 and association of D.A. to GRK 2213, this study would not have been possible.

References

Allingham JS, Smith R, Rayment I. 2005. The structural basis of blebbistatin inhibition and specificity for myosin II. *Nat Struct Mol Biol* 12:378–379.

Anton-Erxleben F, Thomas A, Wittlieb J, Fraune S, Bosch TC. 2009. Plasticity of epithelial cell shape in response to upstream signals: a whole-organism study using transgenic *Hydra*. *Zoology (Jena)* 112:185–194.

Aufschnaiter R, Zamir EA, Little CD, Ozbek S, Munder S, David CN, Li L, Sarras MP Jr, Zhang X. 2011. In vivo imaging of basement membrane movement: ECM patterning shapes *Hydra* polyps. *J Cell Sci* 124:4027–4038.

Beckmann A, Ozbek S. 2012. The nematocyst: a molecular map of the cnidarian stinging organelle. *Int J Dev Biol* 56:577–582.

Bland JM, Altman DG. 1996. Statistics notes. Logarithms. *BMJ* 312:700.

Blankenship JT, Backovic ST, Sanny JS, Weitz O, Zallen JA. 2006. Multicellular rosette formation links planar cell polarity to tissue morphogenesis. *Dev Cell* 11:459–470.

Bottger A, Doxey AC, Hess MW, Pfaller K, Salvenmoser W, Deutzmann R, Geissner A, Pauly B, Altstatter J, Munder S, Heim A, Gabius HJ, McConkey BJ, David CN. 2012. Horizontal gene transfer contributed to the evolution of extracellular surface structures: the freshwater polyp *Hydra* is covered by a complex fibrous cuticle containing glycosaminoglycans and proteins of the PPOD and SWT (sweet tooth) families. *PLoS One* 7:e52278.

Bottger A, Hassel M. 2012. *Hydra*, a model system to trace the emergence of boundaries in developing eumetazoans. *Int J Dev Biol* 56:583–591.

Boureux A, Vignal E, Faure S, Fort P. 2007. Evolution of the Rho family of ras-like GTPases in eukaryotes. *Mol Biol Evol* 24: 203–216.

Burute M, Thery M. 2012. Spatial segregation between cell-cell and cell-matrix adhesions. *Curr Opin Cell Biol* 24:628–636.

Buzgariu W, Al Haddad S, Tomczyk S, Wenger Y, Galliot B. 2015. Multi-functionality and plasticity characterize epithelial cells in *Hydra*. *Tissue Barriers* 3:e1068908.

Chapman JA, Kirkness EF, Simakov O, Hampson SE, Mitros T, Weinmaier T, Rattei T, Balasubramanian PG, Borman J, Busam D, Disbennett K, Pfannkoch C, Sumin N, Sutton GG, Viswanathan LD, Walenz B, Goodstein DM, Hellsten U, Kawashima T, Prochnik SE, Putnam NH, Shu S, Blumberg B, Dana CE, Gee L, Kibler DF, Law L, Lindgens D, Martinez DE, Peng J, Wigge PA, Bertulat B, Guder C, Nakamura Y, Ozbek S, Watanabe H, Khalturin K, Hemmrich G, Franke A, Augustin R, Fraune S, Hayakawa E, Hayakawa S, Hirose M, Hwang JS, Ikeo K, Nishimiya-Fujisawa C, Ogura A, Takahashi T, Steinmetz PR, Zhang X, Aufschnaiter R, Eder MK, Gorny AK, Salvenmoser W, Heimberg AM, Wheeler BM, Peterson KJ, Bottger A, Tischler P, Wolf A, Gojobori T, Remington KA, Strausberg RL, Venter JC, Technau U, Hobmayer B, Bosch TC, Holstein TW, Fujisawa T, Bode HR, David CN, Rokhsar DS, Steele RE. 2010. The dynamic genome of *Hydra*. *Nature* 464:592–596.

Dailey L, Ambrosetti D, Mansukhani A, Basilico C. 2005. Mechanisms underlying differential responses to FGF signaling. *Cytokine Growth Factor Rev* 16:233–247.

Fagotto F. 2014. The cellular basis of tissue separation. *Development* 141:3303–3318.

Fagotto F, Rohani N, Touret AS, Li R. 2013. A molecular base for cell sorting at embryonic boundaries: contact inhibition of cadherin adhesion by ephrin/ Eph-dependent contractility. *Dev Cell* 27:72–87.

Foley KS, Young PW. 2014. The non-muscle functions of actinins: an update. *Biochem J* 459:1–13.

Graf L, Gierer A. 1980. Size, shape and orientation of cells in budding *Hydra* and regulation of regeneration in cell aggregates. *Wihelm Roux Arch Dev Biol* 188:141–151.

Grens A, Gee L, Fisher DA, Bode HR. 1996. CnNK-2, an NK-2 homeobox gene, has a role in patterning the basal end of the axis in *hydra*. *Dev Biol* 180:473–488.

Guglielmi G, Barry JD, Huber W, De Renzis S. 2015. An optogenetic method to modulate cell contractility during tissue morphogenesis. *Dev Cell* 35:646–660.

Harding MJ, Nechiporuk AV. 2012. Fgfr-Ras-MAPK signaling is required for apical constriction via apical positioning of Rho-associated kinase during mechanosensory organ formation. *Development* 139:3130–3135.

Hasse C, Holz O, Lange E, Pisowodzki L, Rebscher N, Christin Eder M, Hobmayer B, Hassel M. 2014. FGFR-ERK signaling is an essential component of tissue separation. *Dev Biol* 395:154–166.

Hassel M, Berking S. 1990. Lithium ions interfere with pattern control in *hydra-vulgaris*. *Roux Arch Dev Biol* 198:382–388.

Hassel M, Bieller A. 1996. Stepwise transfer from high to low lithium concentrations increases the head-forming potential in *Hydra vulgaris* and possibly activates the PI cycle. *Dev Biol* 177:439–448.

Hobmayer B, Jenewein M, Eder D, Eder MK, Glasauer S, Gufler S, Hartl M, Salvenmoser W. 2012. Stemness in *Hydra* - a current perspective. *Int J Dev Biol* 56:509–517.

Hobmayer B, Rentsch F, Kuhn K, Hoppel CM, von Laue CC, Snyder P, Rothbacher U, Holstein TW. 2000. WNT signalling molecules act in axis formation in the diploblastic metazoan *Hydra*. *Nature* 407:186–189.

Jeanmougin F, Thompson JD, Gouy M, Higgins DG, Gibson TJ. 1998. Multiple sequence alignment with Clustal X. *Trends Biochem Sci* 23:403–405.

Kovacs M, Toth J, Hetenyi C, Malnasi-Csizmadia A, Sellers JR. 2004. Mechanism of blebbistatin inhibition of myosin II. *J Biol Chem* 279:35557–35563.

Kroening S, Stix J, Keller C, Streiff C, Goppelt-Struebe M. 2010. Matrix-independent stimulation of human tubular epithelial cell migration by Rho kinase inhibitors. *J Cell Physiol* 223:703–712.

Lange E, Bertrand S, Holz O, Rebscher N, Hassel M. 2014. Dynamic expression of a *Hydra* FGF at boundaries and termini. *Dev Genes Evol* 224:235–244.

Levayer R, Lecuit T. 2012. Biomechanical regulation of contractility: spatial control and dynamics. *Trends Cell Biol* 22:61–81.

- Martin AC, Goldstein B. 2014. Apical constriction: themes and variations on a cellular mechanism driving morphogenesis. *Development* 141:1987–1998.
- Martin AC, Kaschube M, Wieschaus EF. 2009. Pulsed contractions of an actin-myosin network drive apical constriction. *Nature* 457:495–499.
- Münder S, Käsbaier T, Prexl A, Aufschnaiter R, Zhang X, Towb P, Böttger A. 2010. Notch signalling defines critical boundary during budding in Hydra. *Dev Biol* 344:331–345.
- Munder S, Tischler S, Grundhuber M, Buchels N, Bruckmeier N, Eckert S, Seefeldt CA, Prexl A, Kasbauer T, Böttger A. 2013. Notch-signalling is required for head regeneration and tentacle patterning in Hydra. *Dev Biol* 383:146–157.
- Nakamura Y, Tsiariris CD, Özbek S, Holstein TW. 2011. Autoregulatory and repressive inputs localize Hydra Wnt3 to the head organizer. *Proc Natl Acad Sci U S A* 108:9137–9142.
- Niehrs C, Pollet N. 1999. Synexpression groups in eukaryotes. *Nature* 402:483–487.
- Otto J, Campbell R. 1977. Budding in Hydra attenuata: bud stages and fate map. *J Exp Zool* 200:417–428.
- Philipp I, Aufschnaiter R, Ozbek S, Pontasch S, Jenewein M, Watanabe H, Rentzsch F, Holstein TW, Hobmayer B. 2009. Wnt/beta-catenin and noncanonical Wnt signaling interact in tissue evagination in the simple eumetazoan Hydra. *Proc Natl Acad Sci U S A* 106:4290–4295.
- Rodrigues M, Ostermann T, Kremeser L, Lindner H, Beisel C, Berezikov E, Hobmayer B, Ladurner P. 2016. Profiling of adhesive-related genes in the freshwater cnidarian Hydra magnipapillata by transcriptomics and proteomics. *Biofouling* 32:1115–1129.
- Rudolf A, Huubinger C, Huusken K, Vogt A, Rebscher N, Oel SF, Renkawitz-Pohl R, Hassel M. 2013. The Hydra FGFR, Kringelchen, partially replaces the Drosophila Heartless FGFR. *Dev Genes Evol* 223:159–169.
- Sarras MP Jr. 2012. Components, structure biogenesis and function of the Hydra extracellular matrix in regeneration, pattern formation and cell differentiation. *Int J Dev Biol* 56:567–576.
- Schenkelaars Q, Quintero O, Hall C, Fierro-Constain L, Renard E, Borchiellini C, Hill AL. 2016. ROCK inhibition abolishes the establishment of the aquiferous system in Ephydatia muelleri (Porifera, Demospongiae). *Dev Biol* 412:298–310.
- Schwayer C, Sikora M, Slovakova J, Kardos R, Heisenberg CP. 2016. Actin Rings of Power. *Dev Cell* 37:493–506.
- Seifert JR, Mlodzik M. 2007. Frizzled/PCP signalling: a conserved mechanism regulating cell polarity and directed motility. *Nat Rev Genet* 8:126–138.
- Seybold A, Salvenmoser W, Hobmayer B. 2016. Sequential development of apical-basal and planar polarities in aggregating epitheliomuscular cells of Hydra. *Dev Biol* 412:148–159.
- Shang X, Marchioni F, Sipes N, Evelyn CR, Jerabek-Willemsen M, Duhr S, Seibel W, Wortman M, Zheng Y. 2012. Rational design of small molecule inhibitors targeting RhoA subfamily Rho GTPases. *Chem Biol* 19:699–710.
- Shimizu H, Aufschnaiter R, Li L, Sarras MP Jr, Borza DB, Abrahamson DR, Sado Y, Zhang X. 2008. The extracellular matrix of hydra is a porous sheet and contains type IV collagen. *Zoology (Jena)* 111:410–418.
- Shimizu H, Zhang X, Zhang J, Leontovich A, Fei K, Yan L, Sarras MP Jr. 2002. Epithelial morphogenesis in hydra requires de novo expression of extracellular matrix components and matrix metalloproteinases. *Development* 129:1521–1532.
- Sjoblom B, Salmazo A, Djinnovic-Carugo K. 2008. Alpha-actinin structure and regulation. *Cell Mol Life Sci* 65:2688–2701.
- Steinmetz PR, Kraus JE, Larroux C, Hammel JU, Amon-Hassenzahl A, Houlston E, Worheide G, Nickel M, Degnan BM, Technau U. 2012. Independent evolution of striated muscles in cnidarians and bilaterians. *Nature* 487:231–234.
- Sudhop S, Coulier F, Bieller A, Vogt A, Hotz T, Hassel M. 2004. Signaling by the FGFR-like tyrosine kinase, Kringelchen, is essential for bud detachment in Hydra vulgaris. *Development* 131:4001–4011.
- Takahashi T, Muneoka Y, Lohmann J, Lopez de Haro M, Solleder G, Bosch T, David C, Bode H, Koizumi O, Shimizu H, Hatta M, Fujisawa T, Sugiyama T. 1997. Systematic isolation of peptide signal molecules regulating development in hydra: LWamide and PW families. *Proc Natl Acad Sci U S A* 94:1241–1246.
- Vasquez CG, Heissler SM, Billington N, Sellers JR, Martin AC. 2016. Drosophila non-muscle myosin II motor activity determines the rate of tissue folding. *Elife* 5.
- Wheeler AP, Ridley AJ. 2004. Why three Rho proteins? RhoA, RhoB, RhoC, and cell motility. *Exp Cell Res* 301:43–49.